ON THE RANGE OF 3D DISLOCATION PAIR CORRELATIONS

F. F. Csikor[1,2], *I. Groma*[1], *T. Hochrainer*[3,4], *D. Weygand*[4], *M. Zaiser*[2]

[1] Department of Materials Physics, Eötvös University, PO Box 32, H-1518 Budapest, Hungary

[2] Centre for Materials Science and Engineering, University of Edinburgh, King's Buildings, Sanderson Building, Edinburgh EH9 3JL, UK

[3] Fraunhofer-Institut für Werkstoffmechanik IWM, Wöhlerstr. 11., 79108 Freiburg, Germany

[4] Institut für Zuverlässigkeit von Bauteilen und Systemen (izbs), University of Karlsruhe, Kaiserstr. 12., 76131 Karlsruhe, Germany

csikor@metal.elte.hu

ABSTRACT: Numerical studies of dislocation pair correlations have played a central role in deriving a continuum theory from the equations of motion of 2D dislocation systems in a mathematically rigorous way. As part of an effort to extend this theory into the full 3D dislocation problem, 3D dislocation pair correlations were studied with discrete dislocation dynamics simulation. As a first approximation, dislocations were modeled as uncharged curves in space (their Burgers vectors were disregarded). An inverse square decay with distance was found to describe the numerically obtained pair correlations of the studied curve system.

Keywords: Continuum theory, Dislocations, Pair correlations, Discrete dislocation dynamics simulation

1 INTRODUCTION

Statistical mechanics studies of discrete 2D systems of straight, parallel edge dislocations have led Groma and co-workers to a rigorously derived prototype continuum model for bridging the micro- and mesoscales of crystal plasticity. Numerical calculation of dislocation pair correlation functions played a crucial part in the construction of the theory [1, 2]: i) The observed short range nature of the correlations (which is nontrivial due to long range elastic dislocation interactions) is a prerequisite for a local theory to exist. ii) Pair correlation functions of homogeneous systems are explicitly present in the theory in the flow stress term as well as in a non-local diffusion-like term which enables the theory to describe size effects.

In current efforts to generalize this theory to the full 3D plasticity problem [3, 4], dislocation pair correlations are expected to play a similar role as in the prototype 2D theory [5]. As there exist no theoretical predictions on the functional form of 3D dislocation correlations, numerical simulation is the obvious means to provide the necessary input for the continuum theory. A pioneering 3D discrete dislocation dynamics (DDD) simulation study [6] considered the deformation of a symmetrically oriented large bcc crystal with periodic boundary conditions and analyzed the simulated dislocation network as a system of randomly distributed curves (in mathematical terms, a stochastic fiber process), disregarding the Burgers vector information. Unfortunately, the single shot approach of this study did not provide enough statistics to get smooth graphs as results and the authors did not connect their numerical results to the crucial theoretical questions mentioned above.

In the present paper, the results of a large number of statistically equivalent DDD simulations are presented. As in [6], the obtained dislocation configurations are analyzed as a system of randomly distributed uncharged curves in space and the radial decay of the pair correlation function of this curve system is studied.

2 SIMULATIONS

The 3D dislocation configurations analyzed below were generated with the DDD code described in [7, 8]. This code is optimized for the small scale plasticity of finite, cuboid-shape fcc single crystals and does not handle periodic boundary conditions. In the model, dislocations are discretized into connected straight segments which are allowed to glide. Junction formation and dislocation annihilation upon contact are also included. Cross slip was turned off in the present simulations to mimic low temperature conditions.

In the following we present the simulated uniaxial tensile deformation of $(0.8\,\mu\mathrm{m})^3$ Al cubes up to an applied strain $\epsilon_{\mathrm{applied}} = 0.67\%$ with an applied strain rate $5000\,\mathrm{s}^{-1}$. The strain rate was chosen just below the quasistatic limit, i.e. above which the measured stress–strain curves started to show enhanced hardening due to inertia effects. To improve angular statistics, the crystals were oriented for [010] symmetric multiple slip. The side faces of the specimens were traction free. At the top and bottom faces displacement boundary conditions were prescribed in the tensile direction whereas the in plane components were traction free, too. The simulations were started with 16 randomly positioned and oriented Frank–Read sources of length $0.22\,\mu\mathrm{m}$ in each slip system, resulting in an initial dislocation density $\rho_{\mathrm{initial}} = 8.3 \times 10^{13}\,\mathrm{m}^{-2}$.

As mentioned in the Introduction, for the present analysis the simulated dislocation configurations were simplified by considering all dislocations and junctions as simple curves in space (their Burgers vectors were disregarded). We then calculated the radial pair correlation function $g(r)$ of these curve systems (see eq. (1) for its definition) which was complicated by three practical problems. i) To get smooth curves as results, we needed to improve the statistics by averaging over an ensemble of identical simulations, different only in their random initial configurations. In the following, an ensemble of 55 simulations is analyzed which proved large enough to smooth out both the average hardening behavior (see fig. 1) and the averaged pair correlation functions (see below). ii) As can be seen in fig. 2, the obtained dislocation configurations were inhomogeneous with dislocation depleted zones near the sample surfaces. The thickness of these zones, around $0.2\,\mu\mathrm{m}$, was found to be roughly equal to the mean dislocation–dislocation distance $1/\sqrt{\rho}$ (see also fig. 1 for volume averaged values of ρ). Despite the different boundary conditions at the top and side cube faces, no visible differences were detected between these two types of dislocation depleted zones. Therefore, in the following we restrict our analysis to the central $(0.4\,\mu\mathrm{m})^3$ sub-volume which proved homogeneous to a good approximation (see fig. 2). iii) The linear size of the studied sub-volume was only four times larger than the mean dislocation–dislocation distance $1/\sqrt{\rho}$. This distorted each obtained pair correlation function $g(r)$ already at distances r where it was still far from its asymptotic value. We corrected for this effect by dividing the measured pair correlation functions with the pair correlation function of a random point distribution in the $(0.4\,\mu\mathrm{m})^3$ sub-volume.

3 DISCUSSION

The radial pair correlation function of a random system of curves can be defined as

$$g(r) = \left(\frac{d}{dr} L(r) \right) / 4\pi r^2 \rho \tag{1}$$

[9] where $L(r)$ is the mean total line length in a sphere of radius r centered at a "typical" curve point and ρ means the line density (total length in a unit volume). In this context, "typical" means that a random choice is made in a way that every point on the curves has the same chance to be chosen. The numerical method to compute $g(r)$ directly followed its definition: i) The entire dislocation network (both mobile dislocations and junctions) was divided into line segments of length 0.5 nm. ii) For every line
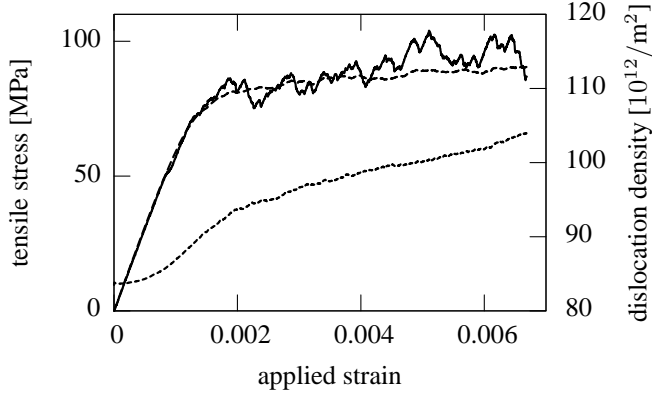
Figure 1: Solid line: typical simulated stress–strain curve. Dashed line: ensemble averaged stress–strain curve. Dotted line: evolution of the ensemble and volume averaged dislocation density.

segment the total curve length was calculated in a sphere of radius r. iii) The curve length values were averaged over all line segments and then substituted into eq. (1) as the numerical estimate for $L(r)$. The results of such a calculation at $\epsilon_{\text{applied}} = 0.67\%$ are displayed in fig. 3 (solid line). (It was found that $g(r)$ depends only slightly on $\epsilon_{\text{applied}}$ and it seems to saturate with increasing $\epsilon_{\text{applied}}$. Further simulations to confirm this up to $\epsilon_{\text{applied}} = 1.3\%$ are in progress). As can be seen in fig. 3, $g(r)$ diverges as r^{-2} as $r \to 0$ and converges to 1 as $r \to \infty$. The main goal of this study is to establish the rate of this convergence. Before this can be done, however, $g(r)$ needs further analysis for two reasons. i) The contiguity of dislocation lines causes strong correlations at small r values. These need to be separated from $g(r)$ as only the correlations between different dislocation lines are interesting for theory [5]. ii) In the simulations, dislocation lines are discretized into linear segments of length 13–66 nm which might also distort the numerically obtained $g(r)$ data. In the following, we analyze $g(r)$ along these problems.

The connected nature of dislocation lines causes two types of strong correlations at small r: i) self correlations of smooth dislocation curves $g_{\text{self}}(r)$ and ii) correlations between different dislocations near their intersections (e.g. arms going out of junctions) $g_{\text{ints}}(r)$. First we analytically calculate the $r \to 0$ asymptotes of these two contributions utilizing eq. (1), then separate them from the numerical $g(r)$ data at small r values to estimate their impact.

As $r \to 0$, $g_{\text{self}}(r)$ is equivalent to the pair correlation function of randomly distributed straight lines with a linear density ρ. We only need that part of the correlation function where a line correlates with itself. From eq. (1) it readily follows that

$$g_{\text{self}}(r) \to 1/2\pi\rho r^2 \text{ as } r \to 0 \tag{2}$$

(the same result was also derived in [9]).

The $r \to 0$ asymptote of $g_{\text{ints}}(r)$ can be modeled with "corners" homogeneously distributed in space. In a "corner" two arms of length l meet at an angle φ and the arms have a linear density ρ. For the $r \to 0$ asymptote of g_{ints}, only that part of the correlation function is interesting where an arm correlates with the arm attached to it. Straightforward calculation from eq. (1) yields

$$g_{\text{ints}}(r) \to \frac{1}{4\pi} \frac{1}{l\rho} \frac{\pi - \varphi}{\sin(\varphi)} \frac{1}{r} \text{ as } r \to 0. \tag{3}$$
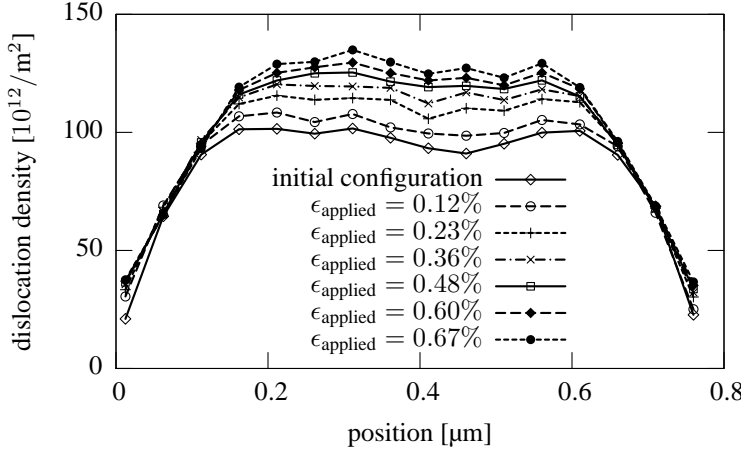
Figure 2: Evolution of the ensemble averaged density profile, averaged over the tensile and one of the perpendicular directions.

Note that in the case of simulated dislocation configurations, averaged l and φ values appear in eq. (3) but this does not affect the r^{-1} character of $g_{\text{ints}}(r)$ at small r.

The next step is assessing the relative contributions of $g_{\text{self}}(r)$ and $g_{\text{ints}}(r)$ to the numerically calculated pair correlation function $g(r)$. To this end, we separated $g(r)$ into three terms utilizing the fact that the simulation code stores dislocation segments organized into loops. The first term, $g_{\text{self}}(r)$, was computed as the correlation function of segment pairs residing on the same loop. The second one, $g_{\text{ints}}(r)$, was calculated as the pair correlation of segment pairs on different loops which touch each other. The last term, $g_{\text{pair}}(r)$, was defined simply as $g(r) - g_{\text{self}}(r) - g_{\text{ints}}(r)$. Fig. 3 displays these three contributions and the total pair correlation function $g(r)$ at $\epsilon_{\text{applied}} = 0.67\%$. Numerical fits of the r^{-2} asymptote of $g_{\text{self}}(r)$ and the r^{-1} asymptote of $g_{\text{ints}}(r)$ at $r \to 0$ are also displayed. Both fit well for $r \lesssim 10$ nm, consistently with the minimum discretization segment length 13 nm, and diverge from the numerical curves at larger distances. Note that $g_{\text{pair}}(r)$ shows no singularity at $r \to 0$, i.e. all connectivity related pair correlation terms were successfully separated. Note also that $g_{\text{pair}}(r) < 1$ (is anticorrelated) and that, to a smaller extent, even $g(r) < 1$ for $r > 0.1$ μm (not visible on the graph). The latter is clearly a finite size effect caused by the independence of $\int_0^\infty g(r) r^2 dr$ from $g(r)$, that $g(r) = 1$ is a valid pair correlation function, and that $g(r) \gg 1$ as $r \to 0$. The authors took the liberty to manually compensate for this effect by adding a small constant $c \ll 1$ to $g(r)$ when analyzing its decay to 1.

We finally study the decay of $g(r)$ towards the uncorrelated value 1 as $r \to \infty$. Fig. 4 depicts $g(r) - 1 + c$ for $\epsilon_{\text{applied}} = 0$ and $\epsilon_{\text{applied}} = 0.67\%$. With $c = 0$ (not shown in the figure), a $g(r) - 1 \propto r^{-2}$ decay can be seen up to $r \approx 20$ nm for $\epsilon_{\text{applied}} = 0$ and $r \approx 30$ nm for $\epsilon_{\text{applied}} = 0.67\%$ before $g(r)$ submerges 1. However, the authors think such an anticorrelated $g(r)$ unlikely. Instead, by carefully adjusting c, an amazingly good fit to r^{-2} can be achieved: at $\epsilon_{\text{applied}} = 0$ with $c = 0.25$ up to $r = 50$ nm and at $\epsilon_{\text{applied}} = 0.67\%$ with $c = 0.08$ up to $r = 100$ nm (1.5 times the discretization segment length 66 nm; see fig. 4). It is clear from fig. 3 that at $\epsilon_{\text{applied}} = 0.67\%$ this r^{-2} decay is not plainly a result of same-loop correlation $g_{\text{self}}(r)$ (cf. eq. (2)) as $g_{\text{self}}(r)$ is 1.5 orders of magnitude smaller than $g(r)$ at $r = 100$ nm. It has also nothing to do with individual straight segments as they are shorter than 66 nm. Therefore, the observed
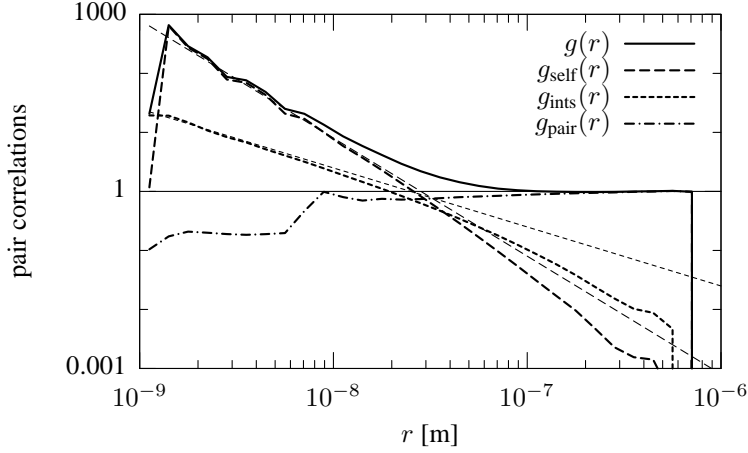
Figure 3: Decomposition of the pair correlation function $g(r)$ at 0.67% applied strain (see text for details). The $r \to 0$ asymptotes of $g_{\text{self}}(r) \propto r^{-2}$ and $g_{\text{ints}}(r) \propto r^{-1}$, and the $r \to \infty$ asymptotes of $g(r) \to 1$ and $g_{\text{pair}}(r) \to 1$ are also indicated.

r^{-2} decay of $g(r)$ is a collective effect at larger distances. This is notable from the point of view that the upper limit of this decay in our simulations, $r = 100$ nm, is still in the range of the mean dislocation–dislocation distance $1/\sqrt{\rho}$ (see fig. 1).
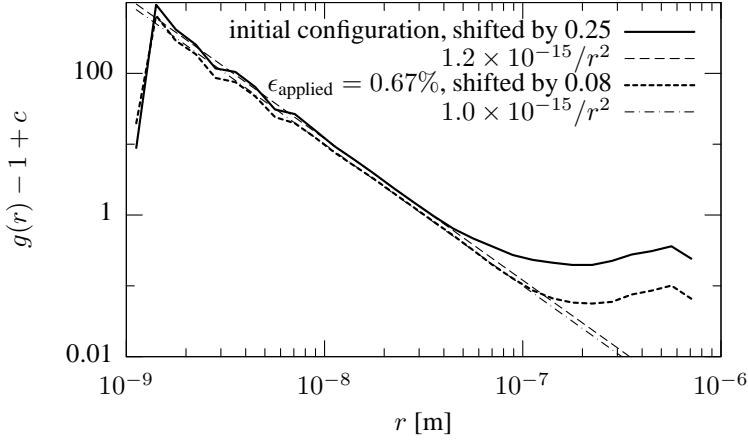

Figure 4: Evolution of the $r \to \infty$ decay of the pair correlation function $g(r)$.

In summary the results indicate a gradual extension of an r^{-2} correlated zone from small r values towards larger ones as the deformation proceeds. A new simulation effort is ongoing to reach $\epsilon_{\text{applied}} = 1.3\%$ for further confirmation.

In a final note, a pair correlation function $\propto r^{-2}$ should be proportional to ρ^{-1} for dimensional reasons. This is consistent with the numerical results in fig. 4 (see also fig. 1 for ρ values).

4 CONCLUSIONS

The correlation properties of 3D many-dislocation systems were studied with discrete dislocation dynamics simulation in symmetrically oriented fcc crystals deformed in uniaxial tension. As a first approximation, dislocation configurations were analyzed as uncharged curve systems in space and the evolution of the corresponding radial pair correlation function was studied. The results indicate the gradual appearance of a pair correlation function $\rho^{-1}r^{-2}$ from small r towards larger ones as the deformation proceeds. Interestingly, this decay is identical to that of 2D systems of infinite, parallel edge dislocations relaxed in multiple slip [10]. Moreover, substituting the numerical result $\rho^{-1}/|\mathbf{r} - \mathbf{r}'|^2$ into eqs. (10–11) in [5] as the double angular integral of d^{pair} suggests that the dimensionless constants denoted by α and $D(\theta)$ in [5] have at most a logarithmic divergence with system size. Whether this divergence is cancelled by the combined angular dependence of g and the dislocation pair interaction τ, enabling finite α and $D(\theta)$ values and thus a local 3D dislocation continuum theory, is the objective of subsequent numerical work.

References

[1] M. Zaiser, M.-C. Miguel, and I. Groma. Statistical dynamics of dislocation systems: The influence of dislocation–dislocation correlations. *Phys. Rev. B*, 64:224102, 2001.

[2] I. Groma, F. F. Csikor, and M. Zaiser. Spatial correlations and higher-order gradient terms in a continuum description of dislocation dynamics. *Acta Mater.*, 51:1271–1281, 2003.

[3] A. El-Azab. Statistical mechanics treatment of the evolution of dislocation distributions in single crystals. *Phys. Rev. B*, 61:11956–11966, 2000.

[4] T. Hochrainer, M. Zaiser, and P. Gumbsch. A three-dimensional continuum theory of dislocation systems: kinematics and mean-field formulation. *Philos. Mag.*, 87:1261–1282, 2007.

[5] M. Zaiser and T. Hochrainer. Some steps towards a continuum representation of 3D dislocation systems. *Scripta Mater.*, 54:717–721, 2006.

[6] A. El-Azab, J. Deng, and M. Tang. Statistical characterization of dislocation ensembles. *Philos. Mag.*, 87:1201–1223, 2007.

[7] D. Weygand, L. H. Friedman, E. Van der Giessen, and A. Needleman. Aspects of boundary-value problem solutions with three-dimensional dislocation dynamics. *Modelling Simul. Mater. Sci. Eng.*, 10:437–468, 2002.

[8] D. Weygand and P. Gumbsch. Study of dislocation reactions and rearrangements under different loading conditions. *Mat. Sci. Eng.*, A 400–401:158–161, 2005.

[9] H. Stoyan and D. Stoyan. Simple stochastic models for the analysis of dislocation distributions. *phys. stat. sol. (a)*, 97:163–172, 1986.

[10] To be published later.